Journal of Controlled Release 133 (2009) 109–118

Contents lists available at ScienceDirect

Journal of Controlled Release

journal homepage: www.elsevier.com/locate/jconrel

Oil-filled polymer microcapsules for ultrasound-mediated delivery of lipophilic drugs

Klazina Kooiman [a,*], Marcel R. Böhmer [b], Marcia Emmer [a], Hendrik J. Vos [a], Ceciel Chlon [b], William T. Shi [c], Christopher S. Hall [c], Suzanne H.P.M. de Winter [b], Karin Schroën [d], Michel Versluis [e], Nico de Jong [a,e,f], Annemieke van Wamel [a]

[a] Department of Biomedical Engineering, Erasmus MC, Rotterdam, The Netherlands
[b] Philips Research Laboratories Eindhoven, Eindhoven, The Netherlands
[c] Philips Research Laboratories North America, Briarcliff Manor, NY, USA
[d] Food and Bioprocess Engineering Group, Department of Agrotechnology and Food Sciences, Wageningen University, Wageningen, The Netherlands
[e] Physics of Fluids Group, University of Twente, Enschede, The Netherlands
[f] Interuniversity Cardiology Institute of the Netherlands, Utrecht, The Netherlands

ARTICLE INFO

Article history:
Received 19 June 2008
Accepted 23 September 2008
Available online 9 October 2008

Keywords:
Ultrasound contrast agent
Polymer-shelled microcapsule
Acoustic properties
Drug delivery
Lipophilic drug

ABSTRACT

The use of ultrasound contrast agents as local drug delivery systems continues to grow. Current limitations are the amount of drug that can be incorporated as well as the efficiency of drug release upon insonification. This study focuses on the synthesis and characterisation of novel polymeric microcapsules for ultrasound-triggered delivery of lipophilic drugs. Microcapsules with a shell of fluorinated end-capped poly(L-lactic acid) were made through pre-mix membrane emulsification and contained, apart from a gaseous phase, different amounts of hexadecane oil as a drug-carrier reservoir. Mean number weighted diameters were between 1.22 μm and 1.31 μm. High-speed imaging at ~10 million fames per second showed that for low acoustic pressures (1 MHz, 0.24 MPa) microcapsules compressed but remained intact. At higher diagnostic pressures of 0.51 MPa, microcapsules cracked, thereby releasing the encapsulated gas and model lipophilic drug. Using conventional ultrasound B-mode imaging at a frequency of 2.5 MHz, a marked enhancement of scatter intensity over a tissue-mimicking phantom was observed for all differently loaded microcapsules. The partially oil-filled microcapsules with high drug loads and well-defined acoustic activation thresholds have great potential for ultrasound-triggered local delivery of lipophilic drugs under ultrasound image-guidance.

1. Introduction

Ultrasound contrast agents (UCA) are routinely used to enhance diagnostic ultrasound (US) imaging. Nowadays, their potential as local drug delivery systems is widely recognised and their use for this purpose continues to expand [1–4]. UCA contain gas microbubbles that are coated by a lipid, protein, sugar, or polymer shell. The diameter of the microbubbles is in the range of 1 to 10 μm [5–7]. The advantage of using them as a drug delivery system is the ability to trigger drug release only at the region of interest. In addition, US imaging of these UCA-based drug delivery systems will aid the guidance and monitoring of therapy [2,4,8].

As with all local drug delivery systems, the aim is to achieve a specific pharmacological response of a therapeutic agent at a particular diseased site in the body. The benefits are a more controlled biodistribution of the therapeutic agent which will not only reduce side-effects, but also improve therapeutic efficacy. This is especially important for therapeutic agents that are very toxic, lack a specific affinity toward a pathological site, or have a low bioavailability because they are rapidly cleared or inactivated by blood components and detoxifying systems [9–12].

In general, two UCA-based drug delivery systems are distinguished. In the first system, the therapeutic agent is co-administered with the UCA so that the UCA circulates through the bloodstream alongside the therapeutic agent. When US is applied locally, endothelial cell membrane permeability will locally and transiently increase and the therapeutic agent will be taken up by the cell or tissue [6,13,14]. In the second system, the therapeutic agent is attached to or incorporated into the microbubbles. Microbubbles of different composition have been designed to carry hydrophilic as well as lipophilic therapeutic agents. When US is applied locally, these microbubbles are triggered to locally release their payload [1,2,4,6,7]. For this type of UCA-based drug delivery system, it is important that the microbubbles: (1) incorporate

* Corresponding author. Department of Biomedical Engineering, Ee2302, Erasmus MC, P.O. Box 2040, 3000 CA Rotterdam, The Netherlands. Tel.: +31 107044036; fax: +31 10 7044720.
E-mail addresses: k.kooiman@erasmusmc.nl (K. Kooiman), marcel.bohmer@philips.com (M.R. Böhmer), j.vanwamel@erasmusmc.nl (A. van Wamel).

0168-3659/$ – see front matter © 2008 Elsevier B.V. All rights reserved.
doi:10.1016/j.jconrel.2008.09.085

an efficient payload of the drug; (2) can be triggered to release the drug with diagnostic US; (3) can be imaged under non-destructive conditions so that US can be used for guidance and monitoring of therapy [2,4,7,14,15]. Loading a sufficient amount of therapeutic agent onto or into a microbubble as well as its efficient release are current limitations for these UCA-based drug delivery systems [7,15].

Instead of incorporating a therapeutic compound into or onto the shell of a microbubble, an additional oil-phase can be incorporated into the microbubbles which increases their lipophilic drug-carrier reservoirs considerably. For lipid-coated microbubbles, this approach has been reported and US-triggered release of the chemotherapeutic drug paclitaxel was demonstrated [16,17]. Using a similar approach, we incorporated an oil-phase in a polymer-shelled UCA. Fluorinated end-capped polymer poly(L-lactic acid), abbreviated as pLA-pFO, was chosen as the shell material. The fluorinated end groups of the pLA-pFO change the surface properties of this biodegradable polymer and make the shell hydrophobic, thereby improving water resistance [18,19]. Hexadecane oil was chosen as drug-carrier reservoir not only because it is non-polar which makes it ideal to solve lipophilic (model) drugs in [20,21], but also because it is a poor solvent for poly(L-lactic acid) [22]. In addition, hexadecane hardly lyophilises during freeze-drying, making it easy to control the amount of oil and drug encapsulation. The aim was to use diagnostic US to release the oil so that the incorporated drug is released from a solution or a fine dispersion rather than through diffusion from the shell of the polymer microbubbles, as the latter has been shown to be inherently slow [23]. Preliminary *in vitro* and *in vivo* studies only suggested the potential of half oil-filled microcapsules as a UCA-based drug delivery system [24]. Important characteristics, such as the acoustic response, the mechanism of US-triggered drug release, and the effect of the amount of encapsulated oil on the acoustic properties were not investigated yet. In this study, we investigate the potential of partially oil-filled microcapsules as UCA-based drug delivery system for lipophilic drugs based on the efficiency to incorporate oil in the microcapsules, the particle size distribution, morphology, acoustic properties, US-triggered drug release, and US imaging capacity.

2. Materials and methods

2.1. Microcapsule preparation

For the polymer microcapsule shell, poly(L-lactic acid) terminated with 1H–1H perfluoro-octan-1-ol (MW 3000), abbreviated as pLA-pFO, was used [18]. The microcapsules were prepared from a 5% (w/w) solution of pLA-pFO in dichloromethane (DCM; Merck, Schiphol, The Netherlands; 1.06050.1000). To 250 mg of this solution, a total of 100 mg of cyclodecane (Fluka, Buchs, Switzerland; 28699) and hexadecane (Sigma-Aldrich, Zwijndrecht, The Netherlands; H6703) were added at a ratio of 1:0 for the production of completely gas-filled microcapsules (S_c), at a ratio 1:1 for the production of half oil-filled microcapsules (S_{ch}), and at a ratio 0:1 for the production of almost completely oil-filled microcapsules (S_h). As a reference sample, solid polymer particles were prepared from the 5% pLA-pFO solution in DCM without the addition of alkanes. The DCM-based solutions were emulsified with 20 g of 0.3% (w/w) poly-vinylalcohol (PVA; Fluka, Buchs, Switzerland; 81383) in water. First, the mix was shaken manually to prepare a premix and then pressed 10 times through an Acrodisk glass filter (1 µm pore size; Gelman, Ann Arbor, MI, USA) for the formation of emulsion droplets. Subsequently, the emulsion was stirred for 1 h to remove the DCM by dissolution in the aqueous phase and subsequent evaporation. After removal of the DCM, a 20% (w/w) poly(ethylene glycol) (PEG, Mw 3000; Sigma-Aldrich, Zwijndrecht, The Netherlands; 20,244-4) solution was added to obtain a total PEG concentration of 5% (w/w) in the suspension. The sample was centrifuged at 3000 rpm (~968 g) for 30 min (Biofuge Stratos, Heraeus, Hanau, Germany). The top fraction was collected and washed two more times in the presence of PEG, after which the sample was filtered over a 13 µm fiber cloth (Kabel Metaal, Zaandam, The Netherlands) and rapidly frozen at −80 °C in a pre-cooled glass vial. To remove the ice and the cyclodecane fraction, freeze-drying took place in an Epsilon 2–6 freeze drier (Martin Christ, Osterode am Harz, Germany) at 1.98 mbar for 20 h and then at 0.03 mbar for another 20 h. After freeze-drying, the apparatus was filled with nitrogen. Lyophilised microcapsules were stored at 4 °C until use, and re-dispersed in 5 ml deionised water for all studies unless mentioned otherwise. The absorbing dye Sudan Black (Sigma-Aldrich, Zwijndrecht, The Netherlands; 199664) is a hydrophobic molecule and was chosen to mimic a lipophilic model drug. For specific experiments, Sudan Black was incorporated into the microcapsules by adding 0.52 mg (S_c and S_h) or 0.26 mg (S_{ch}) Sudan Black to the 5% (w/w) solution of pLA-pFO in DCM during the microcapsule preparation.

2.2. Composition of microcapsules

2.2.1. Modulated differential scanning calorimetry (MDSC)

For the determination of the microcapsule composition by MDSC, the microcapsule preparation was carried out without PEG since it affects the MDSC analysis. As the only function of PEG is to get rapid re-dispersion of the microcapsules, it is not needed for the MDSC analysis. MDSC experiments were performed using a Q1000 calorimeter (TA-instruments, New Castle, DE, USA). For the analysis, lyophilised microcapsules and the pLA-pFO polymer were weighed (~0.5 mg) on an MX5 precision balance (Mettler Toledo, Tiel, The Netherlands) and then packed in Perkin-Elmer aluminium pans (Groningen, The Netherlands). Empty reference pans were included. A modulated heating program was used. The temperature of the pans was first equilibrated at −50 °C. The heating cycle started from this point until 200 °C at a rate of 5 °C/min. The amplitude of the modulation was 1 °C at a period of 60 s. The MDSC program used here is similar to other programs found in the literature for the analysis of poly(lactic acid) microspheres [25,26] and fibers [27].

2.2.2. Gas chromatography/mass spectrometry (GC/MS)

To quantify hexadecane inclusion in the microcapsules, GC/MS was performed. For this analysis, the microcapsule preparation procedure was carried out without the addition of PEG, as in the MDSC experiments. An Agilent 6890 Gas Chromatograph with a 5973N quadrupole Mass Spectrometer (Amstelveen, The Netherlands) was used. Lyophilised microcapsules dissolved in DCM (at a concentration of ~0.5 mg/ml) were injected, using a CTC CombiPAL sample robot (Zwingen, Switzerland), into a split/splitless injector. In split mode, 1 µl was injected (1:150) at 300 °C. Compounds were separated on a Varian-Chrompack VF1-MS column (30 m × 0.25 mm I.D. × 0.25 µm film). The carrier gas was helium at a flow rate of 1.0 ml/min. The oven temperature of 80 °C was ramped to 240 °C at 20 °C/min, followed by a ramp of 10 °C/min to 300 °C, and held at 300 °C for 2 min. Spectra were recorded using electron impact (EI) ionisation with nominal electron energy of 70 eV. The scan range was m/z 29–400. The temperature of the mass spectrometer source was set at 230 °C and the quadrupole was set at 150 °C. Measurements were done in triplicate. Calibration curves ($n=3$) were prepared with known concentrations of cyclodecane and hexadecane diluted in DCM, yielding linear regression coefficients of $R^2 > 0.999$.

2.2.3. Gas encapsulation

The amount of encapsulated gas in the microcapsules was determined with oscillating U-tube densitometry with a DMA 5000 (Anton Paar, Graz, Austria) as reported previously [28,29]. First, the density of the re-dispersed microcapsules was measured in triplicate (microcapsule concentration was ~1% v/v). Then, 5 ml of re-dispersed microcapsules were sonicated for 30 s with a Sonifier 250 (microtip, output level 5; Branson, Danbury, CT, USA) to destroy the microcapsules and thereby remove the encapsulated gas. Thereafter, density was measured again in triplicate. The encapsulated gas fraction (% v/v) was

calculated using $(\rho_{\text{aftersonication}} - \rho_{\text{before sonication}})/(\rho_{\text{aftersonication}} - \rho_{\text{air}})$. The encapsulated gas fraction per microcapsule (in %) was calculated by dividing the encapsulated gas fraction by the volume of the microcapsules: $\frac{4}{3}\pi N \sum_{i=1}^{k} x_i r_i^3$, where x_i is the number fraction, r_i the radius of that fraction, and k the number of bins (as determined with the Coulter Counter).

2.2.4. Microcapsule size distribution

Microcapsule size distributions were measured (n=3) on a Coulter Counter Multisizer 3 (Beckman Coulter, Mijdrecht, The Netherlands). A 20 μm aperture tube was used, allowing quantification between 0.40 and 12 μm using a linear spacing between the 256 channels. Size distributions were determined before and after the microcapsules were freeze-dried. To assess the polydispersity of the samples the SPAN was calculated, which illustrates the width of the distribution, by using (d90%–d10%)/d50% where d90, d10 and d50 are the microcapsule diameters below which 90, 10, and 50% of the cumulative amount of microcapsules is found.

2.2.5. Transmission electron microscopy (TEM) and scanning electron microscopy (SEM)

TEM was used to obtain an impression of microcapsule shell thickness and to determine whether they contained gas and/or oil. Samples were prepared by applying lyophilised microcapsules onto standard TEM grids (C foil on Cu grid; Agar formvar/carbon films, Stansted, UK). TEM studies were performed using a CM12 system (Philips, Eindhoven, The Netherlands), operating at 120 kV in low-dose mode. SEM was used to evaluate the surface structure of the microcapsules. Samples were prepared by applying a drop of re-dispersed microcapsules on a silica substrate. Samples were dried and SEM studies were performed using a SEM XL 40 FEG system (Philips, Eindhoven, The Netherlands).

2.3. Acoustic properties of the microcapsules

2.3.1. Attenuation

Ultrasonic properties of the microcapsules and solid polymer particles were determined *in vitro* by measuring the attenuation as a function of frequency. A pulse-echo set-up was employed using the back wall of the sample chamber as a reflector. In a water tank, four focused single element transducers (V305, centre frequency of 2.5 MHz; V308, centre frequency of 5 MHz; V319, centre frequency of 15 MHz; and V317, centre frequency of 20 MHz; Panametrics-NDT™, Olympus NDT, Waltham, MA, USA) were mounted in parallel to allow attenuation measurements from 0.3–22 MHz on the same sample. The back wall of the sample chamber was positioned in the focus of the transducers. To obtain sufficient attenuation of the microcapsules and solid polymer particles, different dilutions in deionised water were applied. S_c and S_{ch} microcapsules were diluted 1:3000 in the 430 ml sample chamber, the S_h microcapsules were diluted 1:1000, and the solid polymer particles were diluted 1:300. A magnetic stirrer was used to ensure a homogeneous distribution of microcapsules. The input of the transducers was 1 cycle of a sine at the centre frequency, which resulted in short pulses with a mechanical index (MI) of 0.033, as was verified by a calibrated hydrophone (0.2 mm PVDF needle hydrophone for the 2.5–15 MHz transducer, 0.075 mm PVDF needle hydrophone for the 20 MHz transducer; both Precision Acoustics Ltd, Dorchester, UK). The difference in received energy before and after the addition of microcapsules or solid polymer particles determined the attenuation by the microcapsules or solid polymer particles. For each transducer, the attenuation was calculated at −20 dB bandwidth around the centre frequency and divided by the acoustic path length. Because attenuation is linearly dependent on the concentration of microbubbles [30], the attenuation could be normalised to a microcapsule or solid polymer particle concentration of 3.5×10^5/ml. Data were smoothed using a power spectral density estimate via Welch's method (8192-point FFT, 64 segments, 70% overlap) (pwelch function in Matlab, Mathworks, Natick, MA, USA).

2.3.2. Event counts

Single microcapsule activation as a function of peak negative acoustic pressure (P_-) was determined using event counts. A description and schematic overview of the set-up is given in reference [31]. Briefly, when the P_- was increased above a certain threshold value, the insonified microcapsules disrupted, which released their gas content. Free gas microbubbles resonate when exposed to US and at the P_- applied, they radiated significant harmonic energy. A microcapsule disruption event was detected and counted when the harmonic energy increased above a defined level (RMS amplitude higher than 2.0 mV). To ensure single microcapsule detection, the microcapsule concentration in the 3.4 l water tank was ~17 microcapsules/ml. For each acoustic pressure, a percentile event count was determined by dividing the number of counted events by the total number of insonifications (n=300). Each percentile event count measurement was repeated independently for at least three times.

2.3.3. Scattering

To determine scattering as function of insonification amplitude in P_- of escaped gas bubbles when single microcapsules cracked upon insonification, the same data as for the event count measurements were used. Scattering, relative to the incident intensity, was calculated by dividing the power of the averaged receive transducer output (in mV) by the power of the transmit transducer input (in mV), which was then normalised to the highest scattering intensity.

2.4. Characterisation of microcapsule behaviour and drug release

2.4.1. Microcapsule behaviour during insonification

Microcapsule behaviour during insonification was studied using the Brandaris 128 high-speed camera system [32]. The experimental set-up was described by for example Emmer et al. [33]. A 1.0 MHz single element transducer (V302; Panametrics-NDT™, Olympus NDT, Waltham, MA, USA) transmitted 10-cycle-sine wave bursts, with P_- ranging from 0.17 to 0.51 MPa (MI=0.17 to 0.51), as verified with a calibrated 0.2 mm PVDF needle hydrophone (Precision Acoustics Ltd, Dorchester, UK). Images of insonified microcapsules were recorded using a 60× water-immersed objective (LUMPlanFI, Olympus, Zoeterwoude, The Netherlands) and 4× magnifier, and recorded in six sequences of 128 image frames at a speed near 10 million frames per second. The time between the sequences was 80 ms. An area–time curve was extracted from the recorded images according to the procedure described in [34]. Images were processed through contrast stretching in Matlab (Mathworks, Natick, MA, USA).

2.4.2. Drug release

Sudan Black release relative to the amount encapsulated was quantified in triplicate for S_c and S_{ch} microcapsules. Lyophilised microcapsules were re-dispersed in 4 ml deionised water and put into a 10 ml syringe. Until the opaqueness markedly changed, microcapsules were compressed by applying pressure to the piston whilst blocking the opening of the syringe by parafilm [29]. The sample was then centrifuged at 500 rpm (Biofuge Stratos, Heraeus, Hanau, Germany). The top fraction (i.e. released fraction) was retrieved (~1 ml), to which 4 g of dodecane (Fluka, Buchs, Switzerland; 44020) was added. Water was added to the remaining fraction to obtain a total volume of 10 ml, and this was centrifuged at 4000 rpm. The bottom fraction (i.e. non-released fraction) was now retrieved, to which 4 g of dodecane was added. Sudan Black was extracted to the dodecane phase for 72 h and absorbance at 560 nm was measured on a FLUOstar microplate reader (BMG Labtech, Offenburg, Germany). As a reference, microcapsules were not compressed. Drug release from a

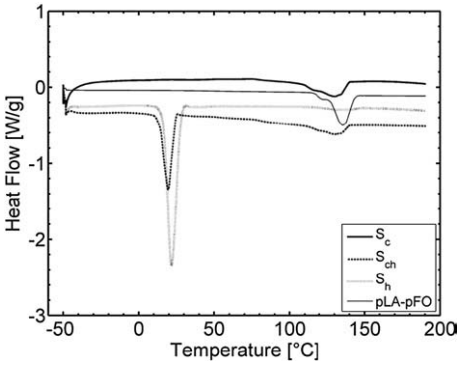

Fig. 1. MDSC thermogram of pLA-pFO and microcapsules re-dispersed after freeze-drying. Given is the heat flow during the heating cycle. The melting peak of hexadecane (18 °C) is clearly visible in the S_{ch} and S_h microcapsules, indicating that these were filled with hexadecane. No melting peak of cyclodecane (9.5 °C) was visible in all three differently loaded microcapsules, indicating that it had successfully been removed in the freeze-drying process.

single microcapsule was also studied using optical recording at video frame rate. The experimental set-up was similar to the one described in Section 2.4.1. However, instead of the Brandaris 128 high-speed camera, a high sensitivity CCD camera (LCL-902K, Watec, Orangeburg, NY, USA) was mounted on top of the microscope. Recordings were taken at 30 frames/s, using a 60× water-immersed objective lens (for S_h microcapsules) (LUMPlanFI, Olympus, Zoeterwoude, The Netherlands) and 2× magnifier (for S_c and S_{ch} microcapsules). Microcapsules were insonified with one burst of a 10 cycle-sine wave at a P_- of 0.51 MPa (MI = 0.51). Images were processed through contrast stretching in Matlab (Mathworks, Natick, MA, USA) and minor pieces of dust on the CCD, not overlapping the microcapsule before and after insonifaction, were removed with the clone brush in Paint Shop Pro 8.

2.5. Ultrasound imaging

To determine the imaging capacity of the microcapsules, *in vitro* diagnostic US imaging was performed. A 2.2 l water tank was filled with water, and a magnetic stirrer was used to ensure a homogeneous distribution of the microcapsules. An acoustic absorbing pad was placed on the bottom of the tank to reduce reflections. On top of this pad, a tissue-mimicking phantom (TMP) was placed (7 cm in diameter, 7 cm in height) that was made of 2% (w/w) agar (CMN 50048, Boom, Meppel, The Netherlands) and 0.2% (w/w) scattering particles (Carborundum No. 600, Cats, Hoogvliet, The Netherlands). Microcapsule suspensions with a final concentration of 1×10^5 capsules/ml, were imaged using a phased array transducer (FPA 2.5 MHz) connected to an echocardiography US system (VingMed System 5; GE, Hoevelaken, The Netherlands). The centre frequency of the transmitted pulses was 2.5 MHz, and the pulse duration was 1.1 μs [35]. Fundamental B-mode images were recorded at two applied power levels: −30 dB and −4 dB. A 0.2 mm PVDF needle hydrophone (Precision Acoustics Ltd, Dorchester, UK) was used to verify that these applied powers corresponded to a P_- of 0.03 MPa (MI = 0.02) and a P_- of 0.53 MPa (MI = 0.51).

3. Results

3.1. Composition of microcapsules

We prepared microcapsules with a cyclodecane to hexadecane ratio of 1:0 for the production of completely gas-filled microcapsules (S_c), at a ratio 1:1 for the production of half oil-filled microcapsules (S_{ch}), and at a ratio 0:1 for the production of almost completely oil-filled microcapsules (S_h). After freeze-drying, the composition of these three differently filled microcapsules were analysed with MDSC, GC/MS and densitometry. The MDSC thermogram is shown in Fig. 1. The absence of a melting peak for cyclodecane at 9.5 °C indicated that cyclodecane had successfully been removed in the freeze-drying process. For the microcapsules filled with hexadecane, a peak was observed at 18 °C, the melting point of hexadecane. This indicated that hexadecane still remained inside these microcapsules after freeze-drying. As the thermal contact for intact gas-filled microcapsules will not be optimal, truly quantitative measurements with MDSC are subject to debate, albeit that we did observe that the hexadecane melting-peak was smaller for the S_{ch} than for the S_h microcapsules. In the thermogram, a melting peak was also observed at 140 °C, which is attributed to melting of crystalline pLA-pFO. This suggested that the shell was at least partly crystalline. This observed peak, however, was much smaller for S_h than for S_c and S_{ch} microcapsules, suggesting that the presence of hexadecane influences the crystallinity of pLA-pFO. To quantitatively determine the amount of hexadecane incorporated in the microcapsules, we performed GC/MS analysis (Table 1). The GC/MS analysis confirmed that cyclodecane was completely removed during the freeze-drying process, while hexadecane was substantially retained. For the S_{ch} microcapsules, which were prepared with a cyclodecane to hexadecane ratio of 1:1, the measured percentage of encapsulated hexadecane was 20% lower than theoretically predicted based on the initial composition. One possible factor for the lowered hexadecane encapsulation efficiency is that during freeze-drying, some of the hexadecane might have sublimed from the microcapsules. Another contributing factor may be that the stabilizer (PVA) was not completely removed during the washing steps, resulting in underestimation of the encapsulation efficiency. If the latter factor is not taken into account, GC/MS revealed that the microcapsules were completely gas-filled (S_c), half-filled with oil (S_{ch}), or almost completely filled with oil (S_h) (Table 1). Density measurements confirmed that the microcapsules contained different amounts of gas (Table 1). Based on these data and a polymer to alkane ratio of 1:8, it could be concluded that the inner core of S_c microcapsules contained ~100 ± 10% gas, for S_{ch} this was 39 ± 1%, and for S_h this was 11 ± 1%.

Fig. 2 shows the size distributions of the S_c, S_{ch}, and S_h microcapsules and the solid polymer particles when they were re-dispersed after freeze-drying. The typical microcapsule concentration was in the order of 1×10^9/ml. For all three differently loaded microcapsules at least 99% of the microcapsules were less than 3.04 μm in diameter. The number weighted mean diameter of the microcapsules ranged between 1.21 and 1.31 μm (Fig. 2), and the volume weighted mean diameter ranged between 2.02 and 2.67 μm, indicating some but limited variation between S_c, S_{ch}, and S_h microcapsules and within batches. This observation was also reflected in the SPAN, as the SPAN was 1.20 for the S_c microcapsules, 1.36 for the S_{ch} microcapsules, and 1.29 for the S_h

Table 1
GC/MS analysis of three types of differently loaded microcapsules when they are re-dispersed after freeze-drying

Sample label	Cyclodecane to hexadecane ratio	% m/m Cyclodecane		% m/m Hexadecane		Encapsulation efficiency (%)	Calculated fill of microcapsules	Encapsulated gas per microcapsule (% v/v)
		Theory	GC/MS	Theory	GC/MS	Hexadecane		
S_c	1:0	0	0 ± 0	0	0 ± 0	–	0% oil	88.8 ± 9.2
S_{ch}	1:1	0	0 ± 0	80	64 ± 4	80 ± 5	40–42% oil	34.9 ± 0.7
S_h	0:1	0	0 ± 0	88	85 ± 1	97 ± 1	97–100% oil	9.7 ± 0.6

Mean values of analysis in triplicate; % m/m are the mass percentages of cyclodecane or hexadecane compared to the mass of the whole microcapsule. Encapsulated gas per microcapsule (% v/v) was determined with densitometry in triplicate.

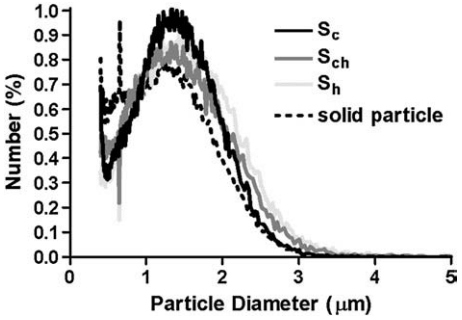

Fig. 2. Coulter counter size distribution measurements of microcapsules and solid polymer particles when re-dispersed after freeze-drying. Number weighted mean diameter (in μm) is 1.21 for S_c, 1.22 for S_{ch}, 1.31 for S_h, and 1.07 for solid polymer. More than 99% of capsules have smaller diameter than (in μm): 2.60 for S_c, 2.88 for S_{ch}, 3.04 for S_h, and 2.57 for solid polymer.

microcapsules. The size of the microcapsules and the width of the distribution were not altered by the freeze-drying process, indicating that the microcapsules were not altered by processing and can be re-dispersed.

Morphology of the microcapsules was studied using electron microscopy. TEM studies revealed that S_c microcapsules were hollow, and had a thin shell of about 40 nm (Fig. 3A). SEM analysis showed that these microcapsules had a spherical shape and an uneven surface (Fig. 3B), which contained pores (Fig. 3C) ranging from 30 to 210 nm. Morphology of S_{ch} and S_h microcapsules could not be studied with TEM and SEM since these microcapsules broke upon introducing them in the vacuum column of the microscopes.

3.2. Acoustic properties of the microcapsules

Attenuation as a function of frequency is presented in Fig. 4A for the S_c, S_{ch}, and S_h microcapsules as well as the solid polymer particles. Attenuation increased with increasing frequency from 0.3 MHz to 15 MHz for the S_c microcapsules and from 0.3 MHz to 10 MHz for the S_{ch} and S_h microcapsules. For each differently loaded microcapsule, the attenuation reached a maximum. For the S_c microcapsules, the maximum attenuation was 0.7 dB/cm at a frequency >15 MHz. The maximum attenuation was 0.4 dB/cm for the S_{ch} microcapsules, and 0.1 dB/cm for the S_h microcapsules at a frequency between 10 and 15 MHz. These maxima show resonant behaviour of these microcapsules and indicate the resonant frequencies, which appeared to decrease with oil encapsulation. The attenuation of the solid polymer particles was ~0 dB/cm over the entire frequency range, indicating that they do not contain gas.

To further characterise the acoustic properties of the microcapsules, percentile event counts from single microcapsules were measured as a function of acoustic pressure. The microcapsules were insonified at a frequency of 1 MHz and the acoustic scattering was detected in the frequency range from 3 to 7 MHz. All three differently loaded microcapsules showed a threshold followed by a sharp increase in event count for increasing P_- (Fig. 4B). To determine the event count threshold, a linear curve was fitted through the measurements having event counts greater than 4%. The intercept with the *x*-axis was taken as the threshold. In this way the threshold for S_c was calculated to be 0.51 MPa, while the threshold of the S_{ch} showed only an insignificant increase to 0.52 MPa. For the S_h microcapsules the threshold was significantly higher, namely 0.65 MPa. The slope of the fitted linear curves above the threshold varied only slightly between the S_c, S_{ch}, and S_h microcapsules, indicating that the activation rates were similar. The percentile event count is proportional to the microcapsule concentration, the confocal region volume, and microcapsule activation rate. Because both the microcapsule concentration and the confocal region volume remained unchanged among all the measurements with the same insonification condition, the percentile event counts therefore are a relative indicator of the percentage of activated microcapsules among all the particles flowing through the confocal region. For a high P_- of 0.8 MPa it can be concluded that about 25% of the S_h microcapsules were activated, while this increased up to 50% for the S_{ch} microcapsules, and up to 65% for the S_c microcapsules. As expected, no event count was shown for the solid polymer particles, suggesting that, although a hydrophobic polymer was used, no gas microbubbles spontaneously adhered to the surface.

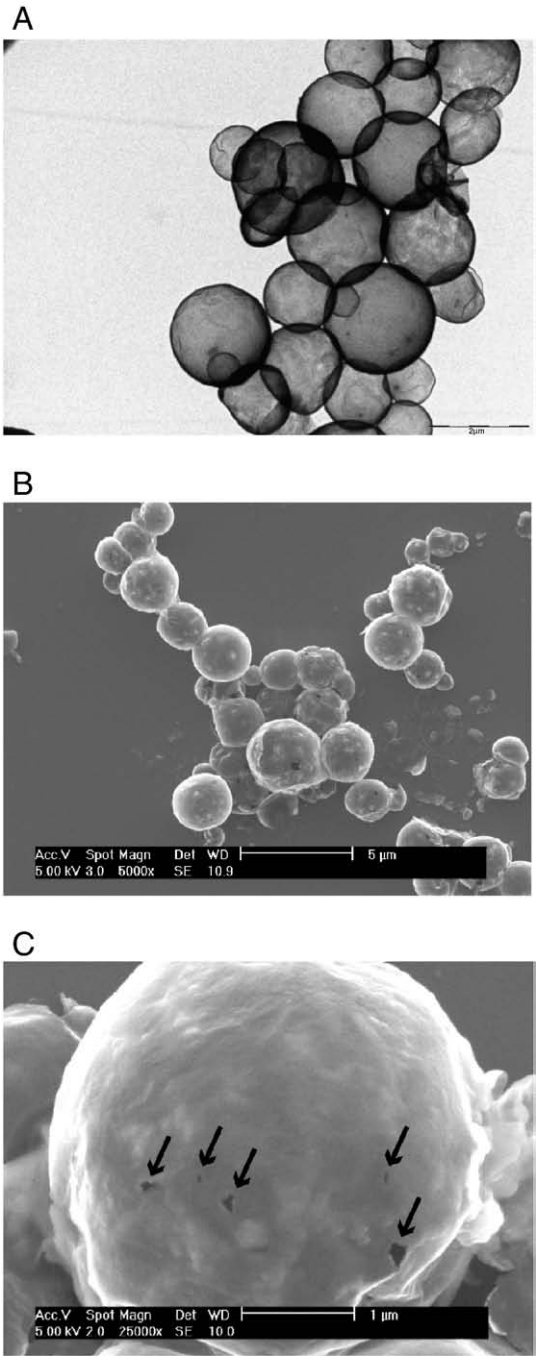

Fig. 3. Electron micrographs of lyophilised S_c microcapsules. A) TEM at 5000 magnification, bar is 2 μm; the microcapsules are hollow and have a thin shell. B) SEM at 5000 magnification, bar is 5 μm; the microcapsules are spherical and have an uneven surface. C) Higher magnification of the microcapsules (SEM at 25,000 magnification, bar is 1 μm), reveals pores in the shell (arrows), ranging from 30 to 210 nm.

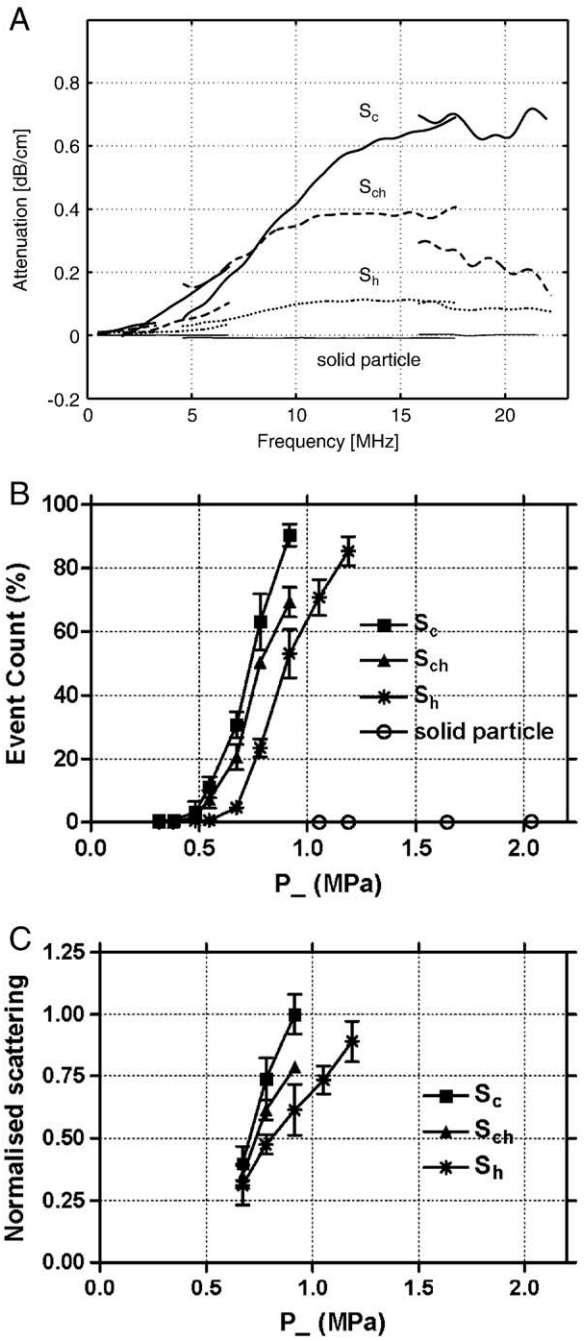

Fig. 4. A) Attenuation (in dB/cm) as function of frequency (0.3–22 MHz) for microcapsules and solid polymer particles. For each differently loaded microcapsule, attenuation reached a maximum. Attenuation of the solid polymer particles was ~0 dB/cm over the entire frequency range. B) Percentile event counts of individual microcapsules when insonified at 1 MHz (signal detected from 3–7 MHz). All three differently loaded microcapsules show a threshold followed by a sharp increase in event count for increasing P_-. The solid polymer particles do not show any event counts. C) Normalised scattering of individual microcapsules when insonified at 1 MHz (signal detected from 3–7 MHz). All three differently loaded microcapsules scatter more with increasing P_-.

Normalised scattering intensity (Fig. 4C) showed that all three differently loaded microcapsules scattered more with increasing P_- when insonified at a frequency of 1 MHz and detected in the frequency range from 3 to 7 MHz. Scattering was highest for the S_c and lowest for the S_h microcapsules, suggesting that the S_c microcapsules contain more gas than the S_{ch} and S_h microcapsules.

3.3. Characterisation of microcapsule behaviour and drug release

Brandaris 128 high-speed camera recordings enabled us to optically observe how individual microcapsules behaved when insonified at a frequency of 1 MHz. At a low MI (P_- of 0.24 MPa; MI=0.24), oil-filled microcapsules typically compressed without shell cracking. An area–time curve of a recording of an S_h microcapsule, 1.6 μm in diameter, is given in Fig. 5A (top panel). During insonification, the area of the

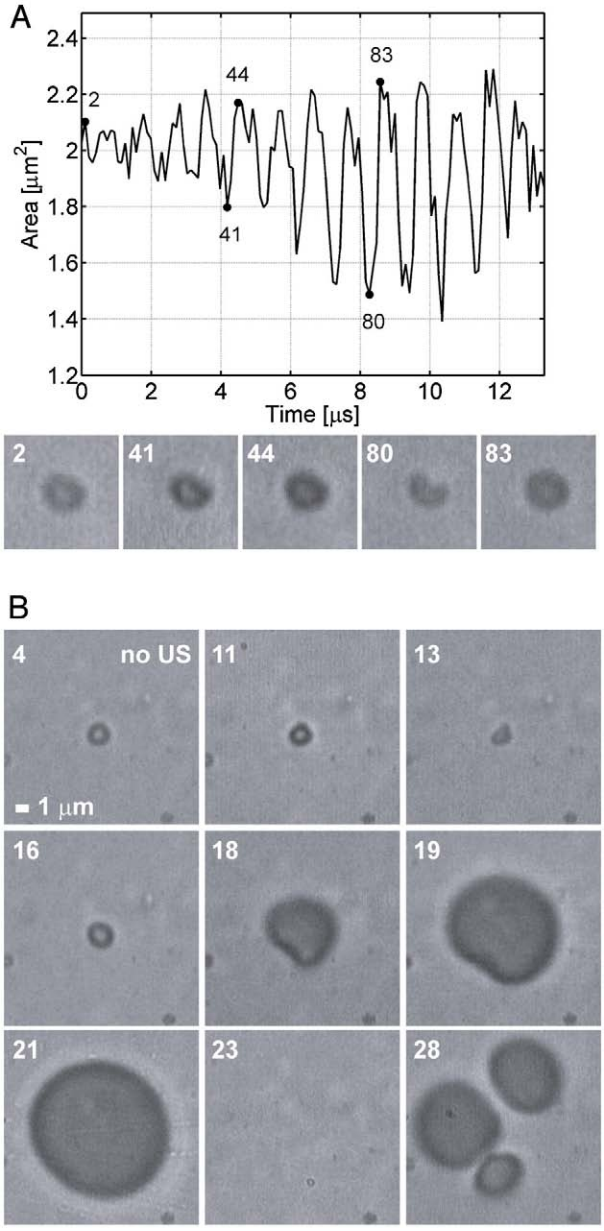

Fig. 5. Brandaris 128 high-speed camera recordings of microcapsules insonified with a 1 MHz transducer. A) Recording at frame rate of 9.56 MHz of an S_h microcapsule, 1.6 μm in diameter, insonified at P_- 0.24 MPa (MI=0.24). Top panel: Area–time curve. Bottom panel: five selected cropped frames (4.5 by 4.5 μm) out of a total of 128 frames showing the microcapsule before insonification (frame #2) and during insonification (frame #41, 44, 80, and 83). Compression but no cracking is observed. B) Recording at frame rate of 9.41 MHz; nine selected cropped frames out of a total of 128 frames of recording of an S_h microcapsule, 1.8 μm in diameter, insonified at P_- of 0.51 MHz (MI=0.51). Frame #4: no ultrasound. Frame #11–13: upon insonification the microcapsule compresses. Frame # 16: microcapsule returns to spherical shape. Frame #18–21: gas escapes from the microcapsule. Frame #23: at the highest pressure of the acoustic cycle the free gas bubble is compressed and not visible. Frame #28: when pressure becomes lower, 3 free gas bubbles are formed.

microcapsule decreased and hardly increased. Compression of the microcapsule was clearly visible in frame #41 and #80 of the bottom panel, and correlated with a positive pressure of the acoustic cycle. The compression was not symmetrical, and can be described as indenting from one side of the microcapsule, which for this particular microcapsule was at the top right corner. Indenting was more pronounced later in the US burst than in the beginning of the US burst. In between compressions, the microcapsule returned to its original spherical shape. These compressions did not crack the microcapsule, as it was still intact in the next recording which was recorded 80 ms later. However, in this next recording, in which the P_- was increased to 0.30 MPa (MI=0.30), this microcapsule did crack after a few more compressions since we observed gas escaping from it at the location where it had indented (data not shown). Similar recordings were made for S_c and S_{ch} microcapsules with indenting occurring at a random place on the microcapsules. Although compression behaviour was identical for the three differently loaded microcapsules, the onset was at different acoustic pressures. About seven times more S_c microcapsules compressed at the lowest P_- of 170 kPa than S_{ch} and S_h microcapsules (n=16–19). Also, about four times more S_c microcapsules cracked at a lower P_- than did S_{ch} and S_h, which is in agreement with the event count measurements shown in Fig. 4B.

When the microcapsules were insonified at a high MI, (P_- of 0.51 MPa; MI=0.51), the microcapsules typically indented only once, leading to cracking or at least weakening of the shell of the microcapsule since in the following negative pressure of the acoustic cycle we observed gas escaping from the microcapsules. Fig. 5B shows nine frames selected out of 128 frames from a typical recording of an S_h microcapsule with a diameter of 1.8 μm (see frame #4). The microcapsule indented (frame #11–13) at a positive pressure and returned to its original spherical shape (frame #16) when the pressure was zero. This was followed by gas escaping from the microcapsule (frame #18–21; negative pressure). The escaped free gas bubble expanded (frame #18–21), collapsed, and expanded again into three free gas bubbles (frame #28). At the peak positive pressures, the free gas bubbles were so compressed that they were no longer visible (frame #23). During the following US cycles, the free gas bubbles continued to expand, collapse, and coalesce. The free gas bubbles were no longer visible in the successive recording which was taken 80 ms later, indicating that they had dissolved. At high MI, the behaviour of the S_c and S_{ch} microcapsules was similar as described for S_h.

For drug release studies, we used microcapsules loaded with Sudan Black. Compressing the microcapsules by applying pressure resulted in a Sudan Black release relative to the amount encapsulated of 38±17% for S_c and 75±6% for S_{ch} microcapsules. MDSC indicated that for S_{ch} microcapsules no pLA-pFO was present in the released top fraction, while the melting peak of hexadecane was detected (data not shown), indicating that this fraction contained the encapsulated material and no intact or fragmented microcapsules. For S_c microcapsules, 64±9% of Sudan Black relative to the amount encapsulated was detected in the bottom fraction while this was 20±10% for S_{ch} microcapsules. Drug release was also triggered using US of 1 MHz at P_- of 0.51 MPa (MI=0.51). Typical video recordings of an S_{ch} and S_h microcapsule showed that the shell of the drug-loaded microcapsules cracked upon insonification, thereby releasing the encapsulated drug (Fig. 6D, F). Shell fragments were identified as wrinkled non-spherical objects. When S_c microcapsules were sonocracked, only the fragmented shell was observed (Fig. 6B).

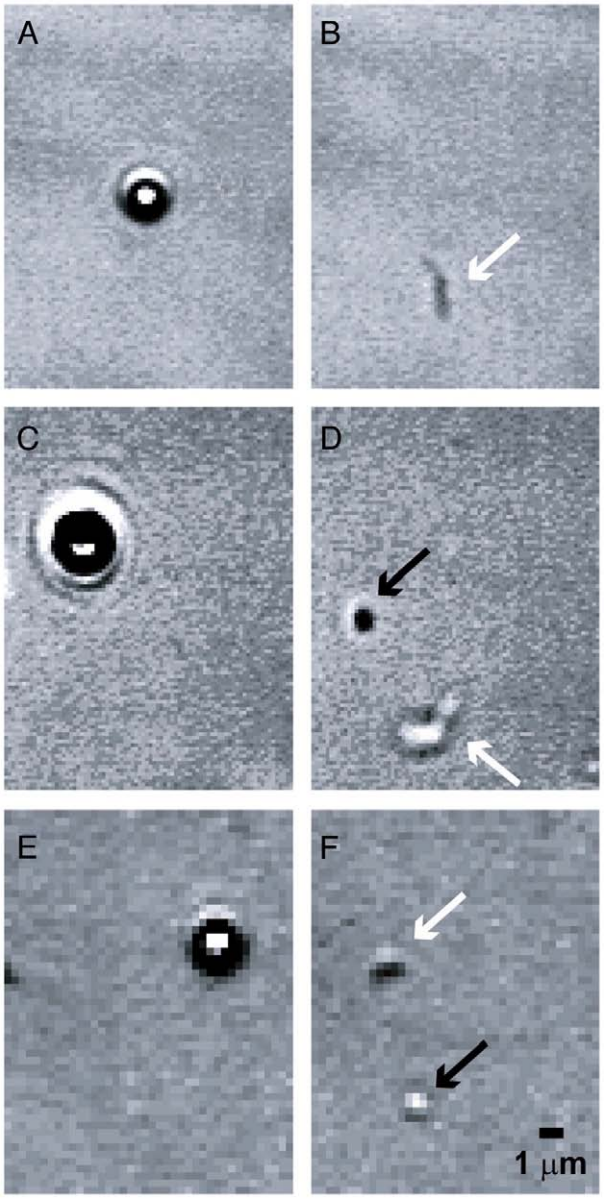

Fig. 6. Selected cropped frames out of typical video recordings of an S_c (A+B; 1.09 μm in diameter), S_{ch} (C+D; 2.08 μm in diameter), and S_h (E+F; 1.76 μm in diameter) microcapsule, loaded with the model lipophilic molecule Sudan Black. A, C, E: microcapsules before insonification. B, D, F: upon insonification at P_- of 0.51 MPa (MI=0.51), the shell fragments (white arrows) and drug is released (black arrows). The selected frames are between 33 and 830 ms after insonification. The shell fragments and released oil droplets have different colours due to the different focal planes.

3.4. Ultrasound imaging

Fig. 7 shows fundamental B-mode images generated by a 2.5 MHz transducer connected to the VingMed System 5. For all suspensions, scattering of the microcapsules was observed when the applied power was 0.03 MPa (MI=0.02) as demonstrated on the left panels of Fig. 7. However, the S_c microcapsules scattered more than the oil-filled microcapsules, which can be attributed to the larger amount of gas in these microcapsules. At this low P_-, no microcapsule destruction is expected since we observed, in both the event count measurements as well as optical observations with the Brandaris-128 high-speed camera, that a much higher P_- was needed to destroy the microcapsules. The right panels of Fig. 7 show B-mode images of the suspensions at a P_- of 0.53 MPa (MI=0.34). The intensities of these images were scaled such that the tissue-mimicking phantom at both acoustic pressures had on average the same intensity. In this way, it can be appreciated that the backscattering at 0.53 MPa was much higher than at 0.03 MPa. At 0.53 MPa (MI=0.34), the microcapsules, independent of their composition, were destroyed and their gas content was released, which resulted in an enhanced backscattering. For all samples, a clear contrast between the microcapsule suspension and the tissue-mimicking phantom was

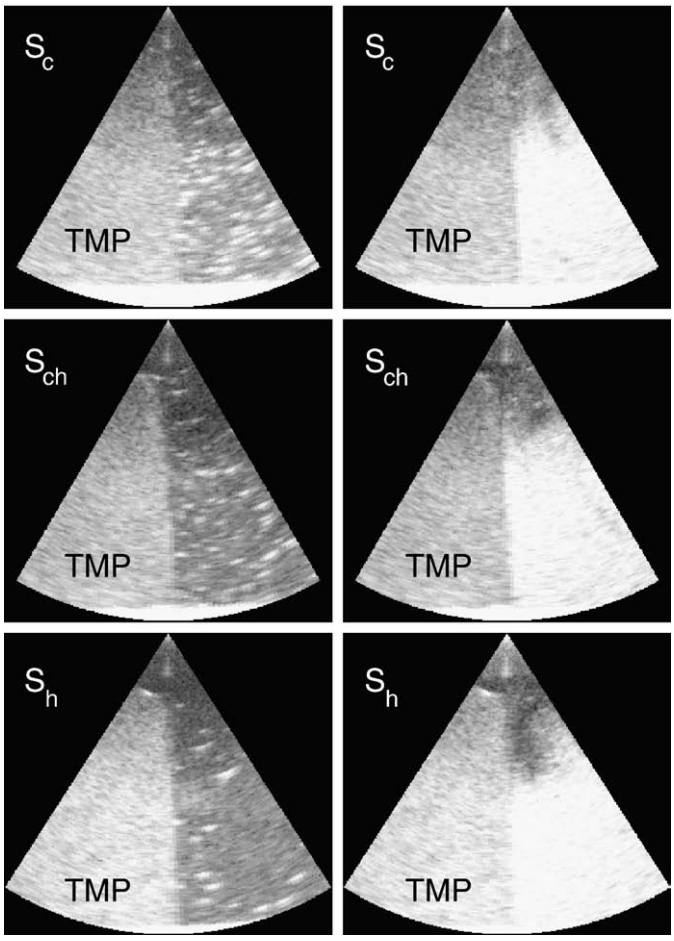

Fig. 7. Fundamental B-mode images recorded with the GE/VingMed System 5 using a 2.5 MHz transducer at a *P*- of 0.03 MPa (MI=0.02; panels on left) and 0.53 MPa (MI=0.34; panels on right). Tissue-mimicking phantom (TMP) is located on the left of the scan; microcapsule suspension is located to the right of the scan. On the lower end of the scans, the lighter region represents the acoustic absorbing pad. Scanconverted image is 9 by 9 cm.

obtained. Fundamental B-mode images made at a centre frequency of 20 MHz, using the Vevo 770 machine (VisualSonics), gave comparable results (data not shown).

4. Discussion

In this study, novel polymer-shelled microcapsules were developed and characterised. The emulsification process used for the synthesis of partly oil-filled microcapsules allowed lipophilic compounds to be incorporated in a straightforward manner by dissolving them in hexadecane. By changing the ratio of cyclodecane to hexadecane, we could make gas-filled (S_c), half-oil filled (S_{ch}), and almost completely oil-filled microcapsules (S_h). The S_h microcapsules were not completely oil-filled and also contained 11±1% gas. Since no cyclodecane was used during emulsification of the S_h microcapsules, the gas must have been incorporated into the microcapsules during another production step. It is likely that this occurred during the freeze-drying process. We found distinct differences between the amount of oil and gas between the S_c, S_{ch}, and S_h microcapsules. Summing the amount of oil and gas for the S_c, S_{ch}, and S_h microcapsules resulted in values rather close to 100% (79–111%).

Although the S_{ch} and S_h microcapsules contained less gas than the S_c microcapsules, the resonance frequency of the S_{ch} and S_h microcapsules was lower than for the S_c microcapsules. This was unexpected since it is known that smaller gas bubbles have higher resonance frequencies than larger gas bubbles [36]. The discrepancy may be explained by the presence of oil and a relatively higher shell to gas ratio which may have increased damping which would result in a lower resonance frequency [37]. In addition, hexadecane may have influenced the pLA-pFO shell as we observed in the MDSC thermogram that the shell was less crystalline when only hexadecane was loaded in the microcapsules. This may have made the shell less rigid which may also have contributed to the lower resonance frequency. Further studies are needed to elucidate this.

As with every drug delivery system, it is important that the system incorporates an efficient payload of therapeutic agent. The pharmaceutical payload per microbubble is limited when drugs are attached to or incorporated into the shell of microbubbles [2]. Hydrophobic drug-carrier reservoirs can be distinctly improved by encapsulation of a liquid oil, for example soybean oil [16] or triacetin oil [38], as reported for acoustically active lipospheres (AALs). Although the S_{ch} and S_h microcapsules described in this study have even larger drug-carrier reservoirs than the AALs, the therapeutic significance of this needs to be investigated and will depend on the amount of drug that can be dissolved in oil and the therapeutic dose that is required. AALs have a relatively wide size range of 1–10 μm in diameter [38], while the S_c, S_{ch}, and S_h have a much narrower size distribution, which is beneficial for controlled drug delivery since a narrower size distribution equals a more defined payload. The near-micrometer size of the pLA-pFO microcapsules also prevents trapping in pulmonary capillaries as well as other capillaries in the body [39]. In addition, AALs have a phospholipid shell and are therefore not believed to be as stable *in vivo* as polymer-shelled UCA [2].

A drug that is not released in the non-target areas of the body, unless the microbubble-drug complex is activated by US, represents the most desirable UCA-based drug delivery system. In addition, US-triggered drug release should be feasible using diagnostic US [2,14,40]. The oil-loaded microcapsules used in this study were typically cracked, thereby triggering drug release, at an MI of 0.34 and 0.51, which is within the clinically safe dose of diagnostic US and can be generated by regular US diagnostic imaging equipment. In comparison, US-triggered drug release from AALs loaded with triacetin is at higher MI's, as values of 0.67 to 2.0 have been reported [17,38,41]. Moreover, AALs loaded with soybean oil were even more difficult to fragment [38]. It is striking that much lower MI's are required to crack our polymer-shelled microcapsules in comparison to most other polymer-shelled microbubbles [42–45]. However, somewhat higher powers were needed to crack S_{ch} and S_h microcapsules compared to S_c microcapsules as illustrated in both the Brandaris 128 high-speed camera studies as well as the event count measurements. Compressing the microcapsules by applying static pressure showed that Sudan Black release is especially efficient for half oil-filled microcapsules since 75±6% of the amount encapsulated was released with the oil. The remaining Sudan Black was retrieved from the bottom fraction, suggesting that it stayed associated with the shell. It needs to be investigated whether this also applies to US-triggered release.

For UCA-based drug delivery systems, it is also important that they can be imaged under non-destructive conditions so that diagnostic US can be used for guidance and monitoring of therapy [4,7]. Our polymer-shelled microcapsules are suited for low MI imaging under non-destructive conditions, which is an important finding. Leong-Poi et al. [46] reported that non-drug loaded microbubbles with a polymer shell made of low molecular weight polylactide could also be used for low-pressure imaging under non-destructive conditions, although they did not investigate how these microcapsules oscillated under non-destructive conditions. How our pLA-pFO microcapsules oscillated under non-destructive conditions was clearly illustrated in the Brandaris 128 high-speed camera studies. At low acoustic pressures, compression-only behaviour was found, which was comparable to behaviour found for the polymer-shelled microsphere PB127 [45].

Unlike other imaging modalities, US can be used to perform triggered, controlled, and local interventions, such as the release of pharmaceutical agents. The minimally invasive nature of US may also permit multiple treatments. Since US systems are portable, bedside

treatment is even possible. On the other hand, there are some limitations as US treatment is only possible in sonographically accessible tissues [1,2,14]. There are also limitations to the novel UCA-based drug delivery system we developed in this study as it can only be used for lipophilic drugs. However, it would be interesting to develop a system with large hydrophilic drug-reservoirs.

Although we have demonstrated US-triggered release with our partially oil-filled microcapsules loaded with Sudan Black, incorporating actual drugs and quantifying their release need to be investigated and will be the focus of our future research. At the same time, preliminary *in vivo* studies with S_{ch} microcapsules loaded with the chemotherapeutic drug paclitaxel were encouraging [24], but further studies also need to be done to demonstrate the therapeutic effect of this novel UCA-based drug delivery system *in vitro* as well as *in vivo*. The biodistribution of the drug-loaded microcapsules as well as the long-term fate of the loaded drug should also be investigated. It is expected that the microcapsules will be taken up by the reticulo-endothelial system (lung, liver, spleen), like reported for polymer microspheres, microparticles, and US contrast agent [47,48]. The possibility therefore exists for increased toxicities to these tissues if the microcapsules contain a toxic drug.

In conclusion, we have made and characterised a novel UCA-based drug delivery system, based on polymer-shelled microcapsules filled with a mixture of gas and oil. Using diagnostic US, we demonstrated the ability to crack the oil-filled microcapsules, thereby releasing the encapsulated gas and drug. In addition, non-destructive imaging of the microcapsules was demonstrated indicating that guidance and monitoring of therapy will be possible. Of the microcapsules studied, the S_h microcapsules had the highest lipophilic drug-reservoir whilst diagnostic US could still be used to trigger drug release. These microcapsules therefore have great potential for US-triggered local delivery of lipophilic drugs.

Acknowledgements

This project is supported by innovation subsidies collaborative projects by the Dutch ministry of economic affairs under nr IS042035. The authors would like to thank Marcel Verheijen (TEM), Hugo Knobel (GC/MS), and Hetty de Barse and Monique Vervest (SEM) from Philips and Ing. Miranda Foppen-Harteveld (Coulter Counter) from the Dept. of Biomedical Engineering, Erasmus MC, for the material analysis. The authors are grateful to Dr. Leonard M. Sagis and Ing. Harry Baptist from the Food Physics Group at Wageningen University for assisting us with the densitometer measurements, and for valuable discussions.

References

[1] W.G. Pitt, G.A. Husseini, B.J. Staples, Ultrasonic drug delivery — a general review, Expert Opin. Drug Deliv. 1 (1) (2004) 37–56.
[2] A.L. Klibanov, Microbubble contrast agents: targeted ultrasound imaging and ultrasound-assisted drug-delivery applications, Invest. Radiol. 41 (3) (2006) 354–362.
[3] P.A. Dijkmans, L.J. Juffermans, R.J. Musters, A. van Wamel, F.J. ten Cate, W. van Gilst, C.A. Visser, N. de Jong, O. Kamp, Microbubbles and ultrasound: from diagnosis to therapy, Eur. J. Echocardiog. 5 (4) (2004) 245–256.
[4] E.C. Unger, T.O. Matsunaga, T. McCreery, P. Schumann, R. Sweitzer, R. Quigley, Therapeutic applications of microbubbles, Eur. J. Radiol. 42 (2) (2002) 160–168.
[5] L.J. Juffermans, P.A. Dijkmans, R.J. Musters, A. van Wamel, A. Bouakaz, F.J. ten Cate, L. Deelman, C.A. Visser, N. de Jong, O. Kamp, Local drug and gene delivery through microbubbles and ultrasound: a safe and efficient alternative for viral vectors? Neth. Heart J. 12 (9) (2004) 398–403.
[6] Y. Liu, H. Miyoshi, M. Nakamura, Encapsulated ultrasound microbubbles: therapeutic application in drug/gene delivery, J. Control. Release 114 (1) (2006) 89–99.
[7] K. Ferrara, R. Pollard, M. Borden, Ultrasound microbubble contrast agents: fundamentals and application to gene and drug delivery, Annu. Rev. Biomed. Eng. 9 (2007) 415–447.
[8] M. Postema, G. Schmitz, Bubble dynamics involved in ultrasonic imaging, Expert Rev. Mol. Diagn. 6 (3) (2006) 493–502.
[9] S. Muro, M. Koval, V. Muzykantov, Endothelial endocytic pathways: gates for vascular drug delivery, Curr. Vasc. Pharmacol. 2 (3) (2004) 281–299.
[10] C.A. Kavanagh, Y.A. Rochev, W.M. Gallagher, K.A. Dawson, A.K. Keenan, Local drug delivery in restenosis injury: thermoresponsive co-polymers as potential drug delivery systems, Pharmacol. Ther. 102 (1) (2004) 1–15.
[11] V.P. Torchilin, Drug targeting, Eur. J. Pharm. Sci. 11 (Suppl 2) (2000) S81–S91.
[12] L.H. Reddy, Drug delivery to tumours: recent strategies, J. Pharm. Pharmacol. 57 (10) (2005) 1231–1242.
[13] A. van Wamel, K. Kooiman, M. Harteveld, M. Emmer, F.J. ten Cate, M. Versluis, N. de Jong, Vibrating microbubbles poking individual cells: drug transfer into cells via sonoporation, J. Control. Release 112 (2) (2006) 149–155.
[14] J.C. Chappell, R.J. Price, Targeted therapeutic applications of acoustically active microspheres in the microcirculation, Microcirculation 13 (1) (2006) 57–70.
[15] R. Bekeredjian, P.A. Grayburn, R.V. Shohet, Use of ultrasound contrast agents for gene or drug delivery in cardiovascular medicine, J. Am. Coll. Cardiol. 45 (3) (2005) 329–335.
[16] E.C. Unger, T.P. McCreery, R.H. Sweitzer, V.E. Caldwell, Y. Wu, Acoustically active lipospheres containing paclitaxel: a new therapeutic ultrasound contrast agent, Invest. Radiol. 33 (12) (1998) 886–892.
[17] M.S. Tartis, J. McCallan, A.F.H. Lum, R. LaBell, S.M. Stieger, T.O. Matsunaga, K.W. Ferrara, Therapeutic effects of paclitaxel-containing ultrasound contrast agents, Ultrasound Med. Biol. 32 (11) (2006) 1771–1780.
[18] M.R. Böhmer, R. Schroeders, J.A.M. Steenbakkers, S.H.P.M. de Winter, P.A. Duineveld, J. Lub, W.P.M. Nijssen, J.A. Pikkemaat, H.R. Stapert, Preparation of monodisperse polymer particles and capsules by ink-jet printing, Colloids Surf., A Physicochem. Eng. Asp. 289 (2006) 96–104.
[19] W.K. Lee, I. Losito, J.A. Gardella, W.L. Hicks, Synthesis and surface properties of fluorocarbon end-capped biodegradable polyesters, Macromolecules 34 (9) (2001) 3000–3006.
[20] D.C. Bloedow, W.L. Hayton, Effects of lipids on bioavailability of sulfisoxazole acetyl, dicumarol, and griseofulvin in rats, J. Pharm. Sci. 65 (3) (1976) 328–334.
[21] P.J. Dowding, R. Atkin, B. Vincent, P. Bouillot, Oil core/polymer shell microcapsules by internal phase separation from emulsion droplets. II: controlling the release profile of active molecules, Langmuir 21 (12) (2005) 5278–5284.
[22] G.H. Ma, Preparation of uniform poly(lactide) microspheres by employing the Shirasu Porous Glass (SPG) emulsification technique, Colloids Surf., A Physicochem. Eng. Asp. 153 (1999) 383–394.
[23] M.S. Romero-Cano, B. Vincent, Controlled release of 4-nitroanisole from poly(lactic acid) nanoparticles, J. Control. Release 82 (1) (2002) 127–135.
[24] W.T. Shi, M. Bohmer, A. van Wamel, M. Celebi, A.L. Klibanov, C.T. Chin, C. Chlon, M. Emmer, K. Kooiman, N. de Jong, C.S. Hall, Ultrasound therapy with drug loaded microcapsules, IEEE Ultrasonics Symposium Proceedings, 2007, pp. 773–776.
[25] J.F. Nijsen, M.J. van Steenbergen, H. Kooijman, H. Talsma, L.M. Kroon-Batenburg, M. van De Weert, P.P. van Rijk, A. De Witte, A.D. Van Schip, W.E. Hennink, Characterization of poly(L-lactic acid) microspheres loaded with holmium acetylacetonate, Biomaterials 22 (22) (2001) 3073–3081.
[26] J.F. Nijsen, A.D. van Het Schip, M.J. van Steenbergen, S.W. Zielhuis, L.M. Kroon-Batenburg, M. van de Weert, P.P. van Rijk, W.E. Hennink, Influence of neutron irradiation on holmium acetylacetonate loaded poly(L-lactic acid) microspheres, Biomaterials 23 (8) (2002) 1831–1839.
[27] S. Solarski, M. Ferreira, E. Devaux, Characterization of the thermal properties of PLA fibers by modulated differential scanning calorimetry, Polymer 46 (25) (2005) 11187–11192.
[28] K. Bjerknes, P.C. Sontum, G. Smistad, I. Agerkvist, Preparation of polymeric microbubbles: formulation studies and product characterisation, Int. J. Pharm. 158 (2) (1997) 129–136.
[29] M. Schneider, P. Bussat, M.B. Barrau, M. Arditi, F. Yan, E. Hybl, Polymeric microballoons as ultrasound contrast agents — physical and ultrasonic properties compared with sonicated albumin, Invest. Radiol. 27 (2) (1992) 134–139.
[30] N. de Jong, L. Hoff, T. Skotland, N. Bom, Absorption and scatter of encapsulated gas filled microspheres: theoretical considerations and some measurements, Ultrasonics 30 (2) (1992) 95–103.
[31] W. Shi, M. Bohmer, S. de Winter, J. Steenbakkers, M. Emmer, A. van Wamel, N. de Jong, C.S. Hall, Ultrasonic characterization of novel monodispersed contrast agents, IEEE Ultrasonics Symposium Proceedings, 2006, pp. 301–304.
[32] C.T. Chin, C. Lancee, J. Borsboom, F. Mastik, M. Frijlink, N. de Jong, M. Versluis, D. Lohse, Brandaris 128: a 25 million frames per second digital camera with 128 highly sensitive frames, Rev. Sci. Instrum. 74 (12) (2003) 5026–5034.
[33] M. Emmer, A. van Wamel, D.E. Goertz, N. de Jong, The onset of microbubble vibration, Ultrasound Med. Biol. 33 (6) (2007) 941–949.
[34] S.M. van der Meer, B. Dollet, M.M. Voormolen, C.T. Chin, A. Bouakaz, N. de Jong, M. Versluis, D. Lohse, Microbubble spectroscopy of ultrasound contrast agents, J. Acoust. Soc. Am. 121 (1) (2007) 648–656.
[35] M. Emmer, H.J. Vos, A. van Wamel, D.E. Goertz, M. Versluis, N. de Jong, Clinical relevance of pressure-dependent scattering at low acoustic pressures, Ultrasonics 47 (1–4) (2007) 74–77.
[36] L. Hoff, P.C. Sontum, J.M. Hovem, Oscillations of polymeric microbubbles: effect of the encapsulating shell, J. Acoust. Soc. Am. 107 (4) (2000) 2272–2280.
[37] T.G. Leighton, The acoustic bubble, Academic Press, London, 1994.
[38] D.J. May, J.S. Allen, K.W. Ferrara, Dynamics and fragmentation of thick-shelled microbubbles, IEEE Trans. Ultrason. Ferroelectr. Freq. Control 49 (10) (2002) 1400–1410.
[39] R.S. Meltzer, E.G. Tickner, R.L. Popp, Why do the lungs clear ultrasonic contrast? Ultrasound Med. Biol. 6 (3) (1980) 263–269.
[40] S.B. Barnett, G.R. Ter Haar, M.C. Ziskin, H.D. Rott, F.A. Duck, K. Maeda, International recommendations and guidelines for the safe use of diagnostic ultrasound in medicine, Ultrasound Med. Biol. 26 (3) (2000) 355–366.
[41] M.J. Shortencarier, P.A. Dayton, S.H. Bloch, P.A. Schumann, T.O. Matsunaga, K.W. Ferrara, A method for radiation-force localized drug delivery using gas-filled lipospheres, IEEE Trans. Ultrason. Ferroelectr. Freq. Control 51 (7) (2004) 822–831.
[42] S. Seemann, P. Hauff, M. Schultze-Mosgau, C. Lehmann, R. Reszka, Pharmaceutical evaluation of gas-filled microparticles as gene delivery system, Pharm. Res. 19 (3) (2002) 250–257.

[43] S.H. Bloch, M. Wan, P.A. Dayton, K. Ferrara, Optical observation of lipid- and polymer-shelled ultrasound microbubble contrast agents, Appl. Phys. Lett. 84 (4) (2004) 631–633.
[44] P.D. Bevan, R. Karshafian, E.G. Tickner, P.N. Burns, Quantitative measurement of ultrasound disruption of polymer-shelled microbubbles, Ultrasound Med. Biol. 33 (11) (2007) 1777–1786.
[45] A. Bouakaz, M. Versluis, N. de Jong, High-speed optical observations of contrast agent destruction, Ultrasound Med. Biol. 31 (3) (2005) 391–399.
[46] H. Leong-Poi, J. Song, S.J. Rim, J. Christiansen, S. Kaul, J.R. Lindner, Influence of microbubble shell properties on ultrasound signal: implications for low-power perfusion imaging, J. Am. Soc. Echocardiogr. 15 (10 Pt 2) (2002) 1269–1276.
[47] J.M. Anderson, M.S. Shive, Biodegradation and biocompatibility of PLA and PLGA microspheres, Adv. Drug Deliv. Rev. 28 (1) (1997) 5–24.
[48] J.A. Straub, D.E. Chickering, T.G. Hartman, C.A. Gloff, H. Bernstein, AI-700 pharmacokinetics, tissue distribution and exhaled elimination kinetics in rats, Int. J. Pharm. 328 (1) (2007) 35–41.